Role of Liquid Indium in the Structural Purity of Wurtzite InAs Nanowires That Grow on Si(111)

ARTICLE *in* NANO LETTERS · NOVEMBER 2014

Impact Factor: 13.59 · DOI: 10.1021/nl502878a · Source: PubMed

NANO LETTERS

Letter

pubs.acs.org/NanoLett

Role of Liquid Indium in the Structural Purity of Wurtzite InAs Nanowires That Grow on Si(111)

Andreas Biermanns,*[,†] Emmanouil Dimakis,[‡,§] Anton Davydok,[†,∥] Takuo Sasaki,[⊥] Lutz Geelhaar,[‡] Masamitu Takahasi,[⊥] and Ullrich Pietsch[†]

[†]University of Siegen, Faculty of Science and Technology, Solid State Physics, 57072 Siegen, Germany

[‡]Paul-Drude-Institut für Festkörperelektronik, 10117 Berlin, Germany

[§]Helmholtz-Zentrum Dresden-Rossendorf, Institute of Ion Beam Physics and Materials Research, 01328 Dresden, Germany

[⊥]Quantum Beam Science Center, Japan Atomic Energy Agency, 1-1-1 Koto, Sayo-cho, Hyogo 679-5148, Japan

ABSTRACT: InAs nanowires that grow catalyst-free along the [111] crystallographic orientation are prone to wurtzite-zincblende polytypism, making the control of the crystal phase highly challenging. In this work, we explore the dynamic relation between the growth conditions and the structural composition of the nanowires using time-resolved X-ray scattering and diffraction measurements during the growth by molecular beam epitaxy. A spontaneous buildup of liquid indium is directly observed in the beginning of the growth process and associated with the simultaneous nucleation of InAs nanowires predominantly in the wurtzite phase. The highly arsenic-rich growth conditions that we used limited the existence of the liquid indium to a short time interval, which is defined as the nucleation phase. After their nucleation, the nanowires grow in the absence of liquid indium, and with a highly defective wurtzite structure. Complementary ex-situ diffuse X-ray scattering measurements and modeling revealed that this structural degradation is due to the formation of densely spaced stacking faults. Thus, high wurtzite phase purity is associated with the presence of liquid indium. This finding implies that pure wurtzite nanowires may be obtained only if the growth is performed under the continuous presence of liquid indium at the growth interface, that is, in the vapor−liquid−solid mode.

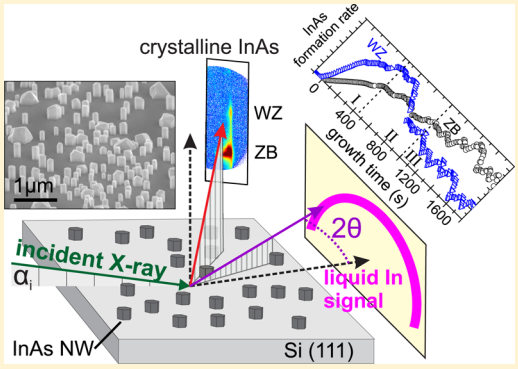

KEYWORDS: *nanowires, InAs, Si, molecular beam epitaxy (MBE), X-ray diffraction*

The epitaxial growth of vertical InAs nanowires (NWs) on Si(111) substrates offers the possibility to integrate monolithically the two semiconductor classes, for example, for novel transistor architectures, maintaining a high quality interface despite of the large mismatch between their lattice constants and thermal expansion coefficients. However, the general susceptibility of III−V NWs to structural polytypism when they are grown along the [111] crystallographic orientation is a major challenge that needs to be resolved for the benefit of any device application.[1] In fact, the coexistence of different polytypes within the same NW can affect basic properties, like the optical transitions[2−5] or the carrier transport.[6,7]

Extensive experimental investigations, also supported by classical nucleation theory models, have shown that it is possible to control the polytypism when the NWs are grown in the Au-assisted, and to a lesser extent in the self-assisted, vapor−liquid−solid (VLS) mode by tuning the supersaturation or the contact angle of the catalyst particle (via the growth conditions).[8−12] In contrast, the freedom to tune the growth energetics in favor of the polytype of choice is limited in the vapor−solid (VS) growth mode, where the (111)B top facet of the NWs ([111]B is the typical growth direction of vertical III−V NWs on Si(111)) is directly exposed to the vapors. The crystal polarity appears to be important here because successful control of the polytypism in VS-grown NWs has been demonstrated only for [111]A oriented InP NWs.[13] Particularly for InAs, the best results have been demonstrated using Au catalyst particles, where phase-pure NWs either zincblende (ZB) or wurtzite (WZ))[14,15] or NWs with zincblende/wurtzite superlattices[16] have been successfully grown. However, when no foreign catalyst is used, InAs NWs can be grown either in the self-assisted VLS[17,18] or the VS[19−22] mode, but in both cases, the structural quality is clearly inferior to the Au-assisted VLS mode. That is, the NWs typically contain a high density of planar stacking faults or twins and both ZB and WZ segments that alternate along the growth axis. Thus, it is highly relevant to develop a better understanding of the polytypism in NWs grown catalyst-free because this is the only way to rule out any possible contamination of the NWs and the substrate crystals

Received: July 27, 2014
Revised: November 7, 2014
Published: November 16, 2014

   dx.doi.org/10.1021/nl502878a | *Nano Lett.* 2014, 14, 6878−6883

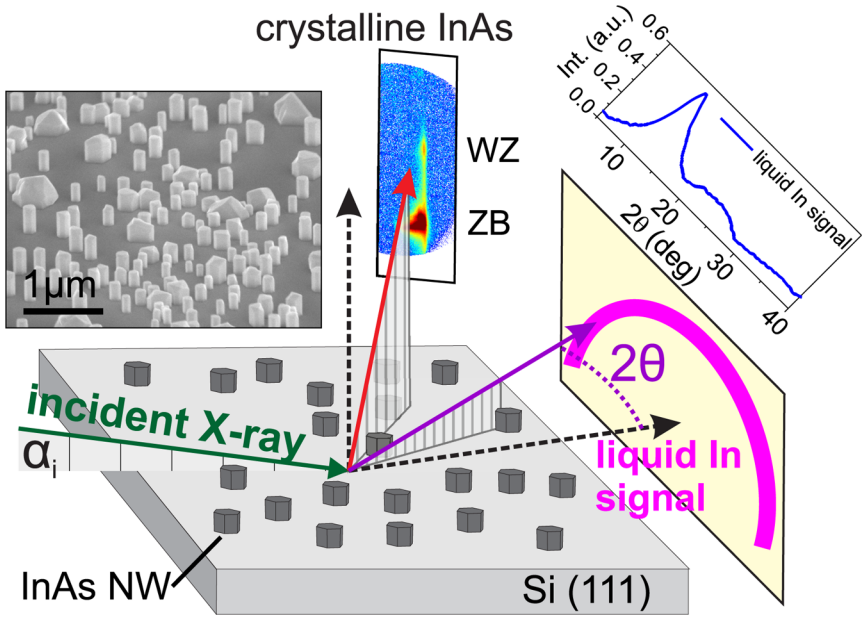

Figure 1. Sketch of the diffraction geometry within the MBE chamber. The incident X-ray beam illuminates the sample surface under a shallow angle of α_i = 0.07°. Liquid indium causes a characteristic, powder-like scattering signal at small scattering angles. Alternatively, the diffraction from crystalline InAs can be observed using a two-dimensional detector. The large extent of the detector allows to simultaneously measure a diffraction signal from the InAs NWs preferentially growing in the wurtzite phase as well as parasitic InAs crystallites growing in the zinc-blende structure. The inset shows an SEM image of the grown NWs and parasitic crystallites after 1800s of growth.

by foreign catalysts like Au, which is a prerequisite for high-performance devices.

In this Letter, we explore the dynamic relation between changes in the local growth conditions and the structural composition of InAs NWs grown catalyst-free on Si(111), in an effort to identify potential ways to achieve phase-pure NWs, particularly in the wurtzite structure. To this end, we developed a procedure to monitor the temporal evolution of the ZB and WZ polytypes as well as the presence of liquid indium (In) during the growth by molecular beam epitaxy (MBE), based on time-resolved X-ray scattering and diffraction measurements. We found that spontaneous transitions of the V/III ratio that take place in localized areas of the substrate surface induce the nucleation of the NWs and determine their structural quality. A more quantitative description of the NW structure was obtained using Monte Carlo simulations of additional ex-situ diffuse X-ray scattering measurements. Altogether, our findings suggest that for phase-pure catalyst-free InAs NWs the local V/III ratio at the growth interface has to be controlled precisely throughout the entire growth process and that the pure wurtzite phase may be obtained only in the VLS growth mode.

Results and Discussion. For the structural characterization of the InAs NWs during growth on Si(111), time-resolved X-ray scattering and diffraction experiments were performed in situ at the synchrotron radiation beamline 11XU at SPring-8 in Japan, using an MBE system integrated with a surface X-ray diffractometer.[23] In order to monitor fast nucleation events with sufficient counting-statistics, we used a sufficiently low growth rate for the InAs NWs. The beam-equivalent pressure for In and As_4 was set to 6.5×10^{-6} Pa and $(2.5-3.0) \times 10^{-4}$ Pa, respectively, corresponding to an equivalent In-limited growth rate for planar InAs (001) of 0.05 monolayers/s. All growth experiments were performed on Si (111) substrates at 400 °C after ex-situ removal of the surface native oxide layer in a HF aqueous solution.

The geometrical configuration of the X-ray measurements is described schematically in Figure 1. The glancing angle of the primary X-ray beam (λ = 0.620 Å, size: 0.3 × 0.3 mm^2) was fixed at α_i = 0.07° with respect to the substrate surface. This angle was set smaller than the critical angle for total external reflection of Si (0.09°) in order to reduce the diffuse scattering from the substrate, whereas the large footprint of the X-ray beam on the surface ensures that a large number of nanowires is illuminated. The X-rays diffracted from crystalline InAs were collected by a 2D-CMOS detector with wide enough acceptance angles (2.7° and 4° in the in-plane and out-of-plane directions, respectively) to measure simultaneously the WZ $(10\bar{1}1)$ and the ZB $(10\bar{1}1)$ signals. Due to the different crystal structures, these reflections are separated in reciprocal space along the direction parallel to the surface normal of the substrate. The small exit angle of the reflected X-ray beam of 5.5° with respect to the substrates surface allows to measure a slice of reciprocal space almost parallel to the surface normal. The two-dimensional imaging was also useful for the separation of the diffraction signal corresponding to InAs nanowires from the background scattering. We were also able to detect if liquid In is formed at any stage of the growth. For that, we performed X-ray scattering measurements placing the detector at smaller scattering angles. As schematically shown in Figure 1, liquid In causes a characteristic powder-like scattering signal at small angles with a maximum at a scattering angle of 2θ = 13° at the used X-ray wavelength, which corresponds to the Fourier transform of the particle distribution function of atoms in the liquid phase.[24] As an example, the 2θ-scan in Figure 1 shows the measured signal of liquid In after a deposition of 10 monolayers of In on a Si substrate. Because only one detector was available in our apparatus, it was not possible to measure the presence of liquid In and the structure of InAs simultaneously during the same growth run, but only in different runs conducted under identical growth conditions.

dx.doi.org/10.1021/nl502878a | Nano Lett. 2014, 14, 6878−6883

The scanning electron microscopy (SEM) inset in Figure 1 illustrates the morphology of a sample grown for 1800 s. The substrate surface is mostly covered by InAs NWs, 300 nm in length and 250 nm in diameter, whereas a few InAs structures of larger diameter and multiple facets (henceforth referred to as parasitic islands) are also present. Figure 2 shows the temporal

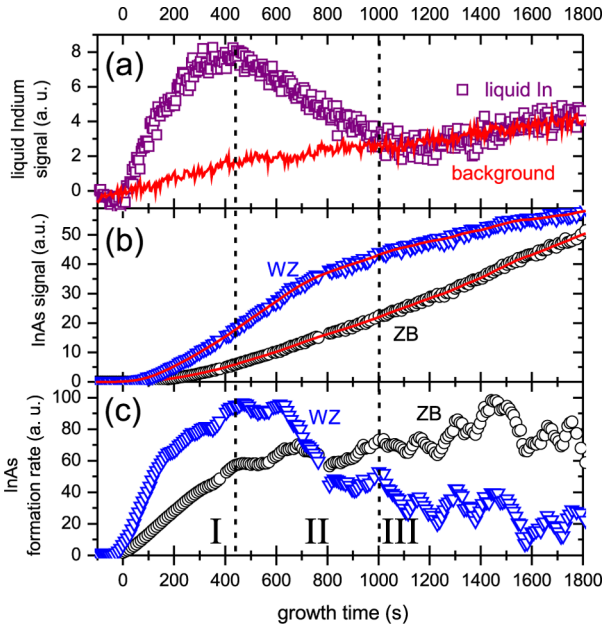

Figure 2. (a) Evolution of the liquid indium signal (open squares) during NW growth, showing a maximum ~440 s after opening the In shutter at $t = 0$ s. (b) Evolution of the crystalline WZ (triangles) as well as the respective ZB signals (open spheres) as a function of growth time. Solid lines represent a running average of the data. (c) Growth rates of ZB and WZ materials, obtained as derivative of the solid lines in (a), showing a good correlation with the liquid In signal.

evolution during the growth of InAs NWs of (a) the scattering signal from liquid In and (b) the diffraction signals from the two polytypes of InAs. The growth started at $t = 0$ s by initiating the supply of In, whereas the supply of As_4 had been initiated several minutes in advance. Despite the As-rich conditions, we detected the formation of liquid In phase during the first 1000 s of the growth. Based on the signal behavior with time, we define three regimes. Regime I is characterized by the monotonic increase of the signal of liquid In, which reaches its maximum at $t \approx 440$ s. Then, the signal drops continuously and eventually diminishes within regime II, following the background-noise level for the rest of the growth duration (regime III). The continuous increase of the background-noise level with time is attributed to the additional material deposited on the substrate.

Under As-rich conditions in MBE, the InAs NWs typically grow on Si substrates in the VS mode.[21,22] Nevertheless, in a previous study, we found indications that the nucleation of InAs NWs must be associated with locally In-rich conditions that form spontaneously on the substrate only in the beginning of the growth.[21] Indeed, our results here confirm the transitional presence of liquid In in the first 1000 s of the growth, which is identified as the nucleation stage. In fact, the detection of liquid In is difficult by any postgrowth experiment because In reacts readily with the residual As_4 that is present in the growth chamber after the growth has been terminated, converting the liquid In into solid InAs.[17,18] The actual role of liquid In in the nucleation of InAs NWs emerges from the study of the structural dynamics of InAs discussed in the following.

Our analysis is mostly focused on the diffraction from the WZ polytype that is exclusively associated with the InAs NWs. In the present experiment the temporal evolution of the diffraction intensity from the WZ polytype exhibited a sigmoidal behavior, that is, a superlinear increase during the first 440 s, followed by a tendency to stabilize for the remaining of the growth [Figure 2b]. Because the diffraction intensity from a given polytype is proportional to the amount of material growing in the respective phase, the formation rate of that polytype can be calculated from the time derivative of the intensity.[25] From the result shown in Figure 2c, we see that the behavior of the WZ formation rate correlates well with the three time regimes that were defined previously for the presence of liquid In. In regime I, the WZ formation rate increases continuously during the first 440 s of the growth, reflecting the increase of the number of InAs NWs that nucleate on the substrate. The formation rate slows down to half of the peak value in regime II, manifesting not only the completion of the nucleation stage, but also the fast degradation of the WZ purity of the growing NWs that were nucleated within regime I. In fact, this structural degradation had already been observed by reflection high energy electron diffraction (RHEED) measurements during growth in our earlier work,[21] where the intensity distribution from structure-sensitive diffraction spots became broader along the ⟨111⟩ crystallographic orientation. In principle, this degradation could mean a decrease in the WZ content in favor of other polytypes within each NW or an increase in the stacking fault density within the WZ segments. Finally, the degradation of the WZ purity of the growing NWs continues throughout regime III, but with a much slower rate than in regime II.

The diffraction signal from the ZB polytype in Figure 2b exhibited a different behavior than the WZ one. This is better illustrated in Figure 2c where the corresponding ZB formation rate is plotted. The formation rate increased monotonically throughout the growth duration, with a faster increase in regime I and a significantly slower one in regimes II and III. The concurrent oscillation of the ZB and WZ formation rates seen in regime II and III is caused most likely by a small fluctuation in intensity of the primary X-ray beam. These fluctuations become prominent when calculating the derivative of scattering intensity as a function of time. With respect to the main trends, safe conclusions about the temporal evolution of the ZB polytype inside the NWs cannot be drawn because the InAs NWs and parasitic islands grow simultaneously on the substrate surface, and they both contain ZB segments. The fast increase of the ZB formation rate within regime I reflects most likely the increasing number of InAs nuclei on the substrate, including in principle both the NWs and the parasitic islands. Nevertheless, the smooth transition of the ZB formation rate between regimes I and II, unlike the WZ peak at 440 s, suggests that the ZB signal in regime I reflects mostly the InAs islands, which nucleate and grow solely in VS mode and for which no decrease of the growth rate is expected at any stage of the growth. The ZB formation rate practically stabilized outside regime I, suggesting that the nucleation phase of the parasitic islands completed at the end of regime I, in coincidence with the nucleation phase of the NWs. That is reasonable because both nucleation mechanisms are diffusion-limited. We have to note that the absolute formation rates of the WZ and the ZB

dx.doi.org/10.1021/nl502878a | Nano Lett. 2014, 14, 6878−6883

polytypes cannot be compared with each other in our experiment. To this end, the integrated intensities of the Bragg reflections would have to be determined, which, however, was not possible in our set up because the measured detector frame represented only a 2-dimensional slice through the reciprocal space.

After all, the comparison between the liquid In and the WZ signals reveals a strong correlation between the presence of liquid In, the nucleation mechanism of InAs NWs, and their structural phase purity. That is, locally In-rich conditions form spontaneously on the substrate in the beginning of the growth and promote the nucleation of InAs in the WZ phase (regime I), whereas the subsequent transition to As-rich conditions defines the end of the nucleation stage (regime II) and accounts for the decrease of the WZ purity in the growing NWs (regimes II and III). All these findings are fully consistent with the model that we already suggested in ref 21, which was based though only on indirect observations. Our model presents some similarities with the VLS growth mode of GaAs NWs concerning the nucleation, which also takes place below spontaneously formed group-III droplets.[26] However, after their nucleation, the InAs NWs grow in a VS mode. Furthermore, our model implies that pure WZ InAs NWs may be grown in the self-assisted way only if the VLS mode is employed. To date, only limited research has been done on the self-assisted VLS growth of InAs NWs;[17,18] thus, WZ NWs with high structural quality have not been demonstrated.

The discussion of our results on the basis of the existing theoretical models for the self-catalyzed VLS growth can be only speculative. According to these models, WZ phase can be formed in VLS-grown GaAs NWs when the gallium droplet has a small enough contact angle with the top NW facet and the nucleation occurs at the triple phase line,[10,12] or when the concentration of arsenic into the gallium droplet (i.e., the supersaturation) is low enough.[11] If we assume that the same scenario holds for the InAs NWs, the WZ phase that we observed in the beginning of the growth may be related to In droplets with low concentration of As (which is reasonable at the early stage of the growth if we assume that the filling rate of the indium droplets with arsenic is slow enough) and possibly small contact angle with the top NW facets. However, obtaining experimental data that could support these speculations would be very challenging. Moreover, we would like to point out that the theoretical models naturally involve parameters whose values are specific for the material system under study. Hence, the microscopic mechanisms may differ for InAs and GaAs NWs.

To shed light on the degradation of the WZ purity in the NWs upon the transition from In-rich to As-rich conditions, additional ex-situ diffraction experiments were conducted at the beamline P08[27] of the PETRAIII synchrotron source in Hamburg, Germany, using experimental conditions with high angular resolution that were not possible for the in situ measurements. Recording complete sections of the reciprocal space rather than a 2-D slice as for the in situ measurements, we were able to determine the concentration of stacking faults in the WZ segments of the NWs. Specifically, we measured the reciprocal space map in the vicinity of phase sensitive X-ray Bragg reflections (see Methods), and extracted the defect-induced angular broadening of the $(10\bar{1}5)$ Bragg reflection of the WZ polytype. Moreover, repeating the measurements for a series of InAs NW samples grown for different durations, it was possible to determine the spatial distribution of the stacking faults along the NW axes and correlate it with the results from the in situ experiments. Table 1 lists the investigated samples

Table 1. Overview of Growth Time, Regime, Length, and Diameter of the NWs Inspected Ex Situ[a]

sample	t_g (s)	R	L (nm)	D (nm)	d_f (nm)
A	5	I–II	30	79	13 ± 1
B	10	I–II	74	88	9 ± 1
C	43	II–III	240	146	8 ± 1
D	86	III	370	119	5.6 ± 1
E	7500	III	5190	202	1.5 ± 1

[a]Growth time, t_g; regime, R; length, L; diameter, D. With increasing NW length, the mean distance between adjacent stacking faults d_f decreases.

(A, B, C, D, and E) and the corresponding mean length and diameter values as obtained from a statistical analysis of scanning electron microscopy (SEM) images. These samples were grown with double flux of In and As_4 compared to the in situ experiments. More details about this series of samples can be found in ref 21. Because the nucleation mechanism and evolution of polytypism that we observed for the in situ measurements described above are consistent with the understanding we deduced in ref 21, it is reasonable to assume that the results to be presented in the following can be used for joint conclusions. For easy comparison with the in situ results, the samples were assigned to the three regimes that we defined in Figure 2 as listed in Table 1. However, the assignment of the samples with the shortest NWs (samples A, B, and C) to regimes I and II cannot be definite because the growth duration of these samples was comparable with the time length of the NW nucleation phase (this is a consequence of the relatively high growth rate that we used).

Figure 3a shows two representative reciprocal space maps (RSM) measured for samples B and E. Here, q_x denotes the momentum transfer parallel to the substrate surface along the $[11\bar{2}]$ direction, whereas q_z measures the momentum transfer parallel to the [111] surface normal, that is, along the NW axis. The probed section of reciprocal space contains two Bragg reflections from the cubic ZB structure, mainly caused by the parasitic islands as we discussed before, as well as the $(10\bar{1}5)$ reflection of the WZ polytype in the NWs.[28] Due to the small differences between the in-plane lattice parameters of ZB and WZ InAs,[29] all reflections line up along a straight line of nearly constant q_x. For a quantitative analysis and comparison of all samples, the data from the RSMs were integrated along the q_x direction, leading to line profiles of integrated intensity along q_z as shown in Figure 3b. The width of the WZ peak does not change significantly in samples A and B, though it increases gradually in samples C, D, and E. This broadening of the reflection is a direct consequence of the increasing density of planar stacking faults within the WZ structure.[30,31] In fact, if the NWs had been grown with pure WZ structure, the diffraction width would have been decreased with increasing growth duration. The ZB reflections have similar intensity as the WZ one in regime I, manifesting the competing nucleation mechanisms of NWs and parasitic islands. In regimes II and III, though, the growth of NWs prevails.

To extract the defect density within the NWs from the line profiles, simulations of the diffracted intensity have been performed within a Monte Carlo approach (see Methods), which was originally developed for the analysis of stacking faults

dx.doi.org/10.1021/nl502878a | Nano Lett. 2014, 14, 6878–6883

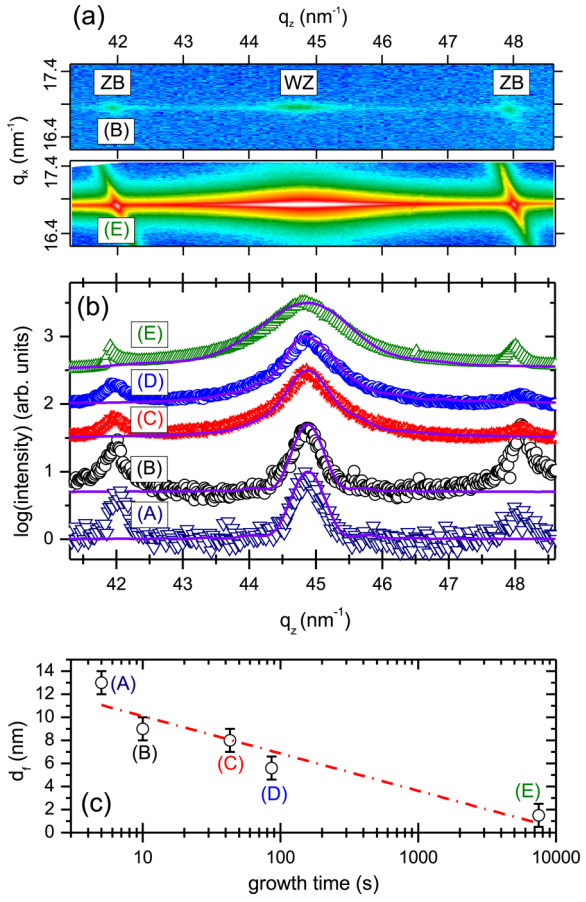

Figure 3. (a) Reciprocal space maps around the WZ ($10\bar{1}5$) reflection for NWs with mean length of 74 nm (B) and 5.2 μm (E), respectively. The strong broadening in (E) indicates a high density of stacking faults. (b) Line profiles obtained from the RSMs in (a) for samples A–E, together with simulations of the defect induced broadening (solid lines). (c) Mean distance between subsequent stacking faults (d_f) as a function of NW growth time. The dash-dotted line is an exponential fit to the data and meant as guide to the eye.

from diffraction patterns of thin films.[31] The NWs are modeled as WZ crystals interrupted by successive stacking faults with a given mean separation distance, d_f. From the best fits to the experimental profiles, plotted as solid lines in Figure 3b, we obtained d_f for all samples. In the simulation process for each sample, the results from the sample with the next shortest NWs were taken into account. As listed in Table 1 and plotted in Figure 3c, d_f decreases rapidly in the beginning of the growth, mostly within the range of regime II, approximating an exponential behavior (dash-dotted line). These results can explain the degradation of the WZ purity that we observed with the in situ measurements, both by XRD as described above and by RHEED as reported in ref.[21] In view of the temporal correlation, the transition from locally In-rich to As-rich conditions is very likely responsible for the onset of the frequent formation of stacking faults.

In conclusion, time-resolved X-ray diffraction measurements during the growth of InAs NWs on Si(111) substrates showed that the nucleation of NWs with WZ structure is associated with the spontaneous formation of liquid In in localized areas of the substrate surface in the beginning of the growth process. Due to the high global V/III flux ratio needed for NW growth, the locally In-rich condition cannot be maintained when the number of nucleated NWs becomes too high, and a sharp transition to locally As-rich conditions sets in. At this point, no new NWs nucleate any more, whereas the already nucleated ones continue to grow with a high density of planar stacking faults. Segments of ZB polytype may form as well under As-rich conditions, but their presence could not be resolved in our experiments. Our model implies that the WZ purity of InAs NWs depends strongly on the local V/III ratio, and the common problem of polytypism may be alleviated when the VLS mode is employed.

Methods. *In-Situ Experiments.* The substrate was cut from a Si (111) wafer having a 100 nm-thick thermally oxidized layer to a size of 20 × 20 × 0.5 mm^3. The oxide layer was removed by chemical etching in 5%-HF solution for 4.5 min so that the hydrogen-terminated Si (111) surface was prepared. The substrate was mounted on a molybdenum block with Ta clamps and transferred to the MBE chamber within 30 min. Prior to the growth of nanowires, the substrate was annealed at 630 °C for 10 min in ultrahigh vacuum. Subsequent InAs nanowire growth was performed at a substrate temperature of 400 °C. An X-ray wavelength of 0.0620 nm (E = 20 keV) was selected using a liquid-nitrogen-cooled Si (111) double crystal monochromator. The size of the X-ray beam was set to 0.3 × 0.3 mm^2 by Rh-coated bent mirrors and Ta-blade slits. The 2D-CMOS detector, PILATUS-100 K (DECTRIS), was placed at a distance of 700 mm from the sample. The diffracted intensity was recorded with a frequency of 1 Hz, and for the sake of visibility, only every fourth data point is shown in Figure 2. To probe the presence of liquid indium, both the intensity at the maximum of the liquid form-factor as well as the background signal were recorded. The signal of crystalline ZB and WZ in Figure 2b corresponds to the relative increase of the integrated intensity of the two diffraction signals on the detector, compared to the initial signal at t = −50 s. The diffracted intensity is proportional to the amount of material in the respective phase. Hence, the temporal derivative of the diffracted intensity is proportional to the growth rates of ZB and WZ materials.[25] To remove the noise from the measured intensity, in a first step a running average of the intensity has been calculated, shown by solid lines in Figure 2b. From this continuous function, the growth rates have been determined and are shown in Figure 2c.

Ex-Situ Experiments. The XRD measurements at NW ensembles were performed at the beamline P08 of the PETRA III synchrotron source in Hamburg.[27] The incoming monochromatic X-ray beam with energy of 9 keV was collimated to a size of 200 × 200 μm^2 using a set of slits in front of the sample. Measurements were performed in a coplanar diffraction geometry with the sample surface mounted horizontally. The diffracted intensity was recorded using a one-dimensional MYTHEN detector aligned along the diffraction angle 2θ, allowing recording of reciprocal space maps within the q_x–q_z plane. Here, the definitions of reciprocal space in the laboratory frame follow the usual conventions with the components of the diffraction vector q_z being parallel to the [111] surface normal, q_x parallel to the projection of the X-ray beam on the surface, and q_y perpendicular to both q_x and q_z.[32] In this configuration, the intensity distribution along the [$10\bar{1}$L] direction in the hexagonal surface coordinate system of the underlying substrate was recorded, accessing a series of structurally sensitive Bragg reflections. In particular the intensities of the (331) and (422) reflections of the cubic zinc-blende phase as well as the ($10\bar{1}5$) reflection of the

dx.doi.org/10.1021/nl502878a | Nano Lett. 2014, 14, 6878–6883

hexagonal wurtzite phase were measured.[28] The width of these reflections along the q_z direction is affected by the presence of stacking faults, allowing to analyze the defect density of the grown nanowires quantitatively.[31] For the simulation, the diffuse scattered intensity in reciprocal space was calculated for a pure wurtzite type nanowire with mean length estimated from SEM images of the respective sample. The stacking fault distribution was modeled assuming a geometric distribution of subsequent stacking fault distances, d_f, appearing within the nanowires. To obtain the ensemble average represented by the measurement, the intensity distribution of 800 different nanowires of same length and different stacking fault arrangements according to the same parameter d_f were averaged. The best estimate for d_f was then obtained by comparison with the experimental data.

AUTHOR INFORMATION

Corresponding Author

*E-mail: andreas.biermanns@uni-siegen.de.

Present Address

[‖]Aix-Marseille Université, Faculté des Sciences, 13397 Marseille, France.

Notes

The authors declare no competing financial interest.

ACKNOWLEDGMENTS

This work was supported by the Deutsche Forschungsgemeinschaft (DFG) under grant Nos. Pi217/38 and Ge2224/2. The authors thank J. Wernecke, O. Seeck, and C. Deiter for support during the ex-situ experiments at beamline P08, PETRA III, V. Holý for support with the X-ray data evaluation, and E. Christalle for the SEM images. The in situ XRD experiments were performed at BL11XU of SPring-8 (Proposals No. 2011B3574 and No. 2013A3503).

REFERENCES

(1) Caroff, P.; Bolinsson, J.; Johansson, J. *IEEE J. Sel. Top. Quantum Electron.* **2011**, *17*, 829−846.

(2) Spirkoska, D.; et al. *Phys. Rev. B* **2009**, *80*, 245325.

(3) Jahn, U.; Lähnemann, J.; Pfüller, C.; Brandt, O.; Breuer, S.; Jenichen, B.; Ramsteiner, M.; Geelhaar, L.; Riechert, H. *Phys. Rev. B* **2012**, *85*, 045323.

(4) Hjort, M.; Lehmann, S.; Knutsson, J.; Timm, R.; Jacobsson, D.; Lundgren, E.; Dick, K. a.; Mikkelsen, a. *Nano Lett.* **2013**, *13*, 4492−8.

(5) Capiod, P.; Xu, T.; Nys, J. P.; Berthe, M.; Patriarche, G.; Lymperakis, L.; Neugebauer, J.; Caroff, P.; Dunin-Borkowski, R. E.; Ebert, P.; Grandidier, B. *Appl. Phys. Lett.* **2013**, *103*, 122104.

(6) Thelander, C.; Caroff, P.; Plissard, S.; Dey, A. W.; Dick, K. a. *Nano Lett.* **2011**, *11*, 2424−9.

(7) Shtrikman, H.; Popovitz-Biro, R.; Kretinin, A. V.; Kacman, P. *IEEE J. Sel. Top. Quantum Electron.* **2011**, *17*, 922−934.

(8) Glas, F.; Ramdani, M. R.; Patriarche, G.; Harmand, J.-C. *Phys. Rev. B* **2013**, *88*, 195304 PRB..

(9) Glas, F.; Harmand, J. C.; Patriarche, G. *Phys. Rev. Lett.* **2007**, *99*, 146101 217UY Times Cited, 86; Cited References Count, 22..

(10) Samsonenko, Y. B.; Cirlin, G. E.; Khrebtov, A. I.; Bouravleuv, A. D.; Polyakov, N. K.; Ulin, V. P.; Dubrovskii, V. G.; Werner, P. *Semiconductors* **2011**, *45*, 431−435 750VA Times Cited, 2; Cited References Count, 16..

(11) Krogstrup, P.; Popovitz-Biro, R.; Johnson, E.; Madsen, M. H.; Nygrd, J.; Shtrikman, H. *Nano Lett.* **2010**, *10*, 4475−4482.

(12) Krogstrup, P.; Curiotto, S.; Johnson, E.; Aagesen, M.; Nyg; aring; rd, J.; Chatain, D. *Phys. Rev. Lett.* **2011**, *106*, 125505.

(13) Ikejiri, K.; Kitauchi, Y.; Tomioka, K.; Motohisa, J.; Fukui, T. *Nano Lett.* **2011**, *11*, 4314−4318.

(14) Shtrikman, H.; Popovitz-Biro, R.; Kretinin, A.; Houben, L.; Heiblum, M.; Bukaa, M.; Galicka, M.; Buczko, R.; Kacman, P. *Nano Lett.* **2009**, *9*, 1506−1510.

(15) Joyce, H. J.; Wong-Leung, J.; Gao, Q.; Tan, H. H.; Jagadish, C. *Nano Lett.* **2010**, *10*, 908−915.

(16) Dick, K. a.; Thelander, C.; Samuelson, L.; Caroff, P. *Nano Lett.* **2010**, *10*, 3494−9.

(17) Mandl, B.; Stangl, J.; Hilner, E.; Zakharov, A. a.; Hillerich, K.; Dey, A. W.; Samuelson, L.; Bauer, G.; Deppert, K.; Mikkelsen, A. *Nano Lett.* **2010**, *10*, 4443−4449.

(18) Rieger, T.; Lepsa, M. I.; SchäPers, T.; Grützmacher, D. *J. Cryst. Growth* **2013**, *378*, 506−510.

(19) Tomioka, K.; Motohisa, J.; Hara, S.; Fukui, T. *Nano Lett.* **2008**, *8*, 3475−80.

(20) Wei, W.; Bao, X.-Y.; Soci, C.; Ding, Y.; Wang, Z. L.; Wang, D. *Nano Lett.* **2009**, *9*, 2926−2934.

(21) Dimakis, E.; Lähnemann, J.; Jahn, U.; Breuer, S.; Hilse, M.; Geelhaar, L.; Riechert, H. *Cryst. Growth Des.* **2011**, *11*, 4001−4008.

(22) Hertenberger, S.; Rudolph, D.; Bolte, S.; Doblinger, M.; Bichler, M.; Spirkoska, D.; Finley, J. J.; Abstreiter, G.; Koblmuller, G. *Appl. Phys. Lett.* **2011**, *98*, 123114.

(23) Takahasi, M.; Yoneda, Y.; Inoue, H.; Yamamoto, N.; Mizuki, J. *Jpn. J. Appl. Phys.* **2002**, *41*, 6247−6251.

(24) Ocken, H.; Wagner, C. N. J. *Phys. Rev.* **1966**, *149*, 122−130.

(25) Krogstrup, P.; Madsen, M. H.; Hu, W.; Kozu, M.; Nakata, Y.; Nygard, J.; Takahasi, M.; Feidenhans'l, R. *Appl. Phys. Lett.* **2012**, *100*, 093103−4.

(26) Colombo, C.; Spirkoska, D.; Frimmer, M.; Abstreiter, G.; Morral, A. F. i. *Phys. Rev. B* **2008**, *77*, 155326.

(27) Seeck, O. H.; Deiter, C.; Pflaum, K.; Bertam, F.; Beerlink, A.; Franz, H.; Horbach, J.; Schulte-Schrepping, H.; Murphy, B. M.; Greve, M.; Magnussen, O. *J. Synchrotron Radiat.* **2012**, *19*, 30−38.

(28) Biermanns, A.; Breuer, S.; Davydok, A.; Geelhaar, L.; Pietsch, U. *Phys. Status Solidi RRL* **2011**, *5*, 156−158.

(29) Kriegner, D.; Panse, C.; Mandl, B.; Dick, K. A.; Keplinger, M.; Persson, J. M.; Caroff, P.; Ercolani, D.; Sorba, L.; Bechstedt, F.; Stangl, J.; Bauer, G. *Nano Lett.* **2011**, *11*, 1483−1489.

(30) Warren, B. *X-ray diffraction*; Dover Publications: New York, 1990.

(31) Barchuk, M.; Hol, V.; Kriegner, D.; Stangl, J.; Schwaiger, S.; Scholz, F. *Phys. Rev. B* **2011**, *84*, 094113 PRB..

(32) Pietsch, U.; Holý, V.; Baumbach, T. *High-Resolution X-Ray Scattering: From Thin Films to Lateral Nanostructures*; Springer: New York, 2004.